X-ray news from the Galactic Center

Enmanuelle Mossoux

LIÈGE université
Astrophysique, Géophysique et Océanographie

25e Congrès Général de la Société Française de Physique

Outline

Outline

The Galactic Center in X-rays

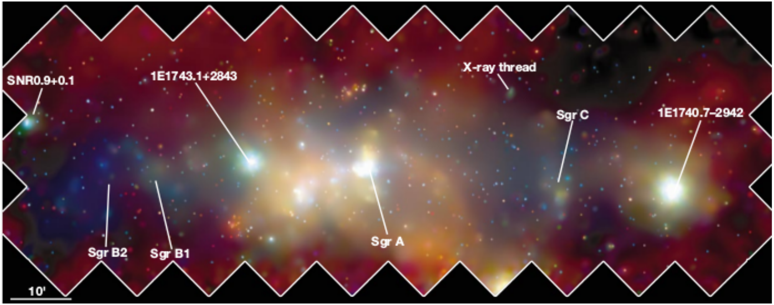

Chandra X-ray survey in 1–8 keV (red = 1–3 keV, green = 3–5 keV and blue = 5–8 keV; Wang et al. 2002)

The Sgr A complex

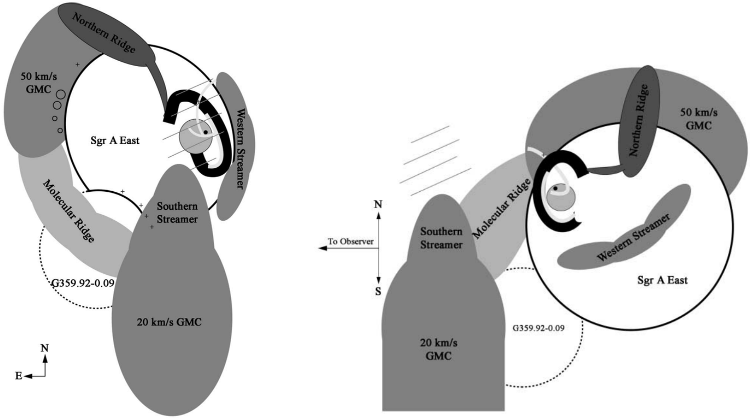

Hornstein et al. (2007)

The Sgr A complex

Old (10^4 years) SNR
Size: $8 \times 10.5\,\mathrm{pc}$
Synchrotron spectrum with $\alpha = -0.76$

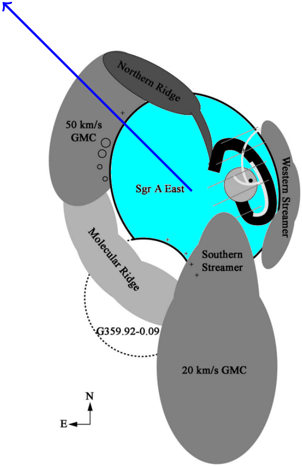

Hornstein et al. (2007)

The Sgr A complex

Sgr A West
Star forming region
Contains luminous stars
rotating at 150 $\mathrm{km\,s^{-1}}$
in a clockwise motion

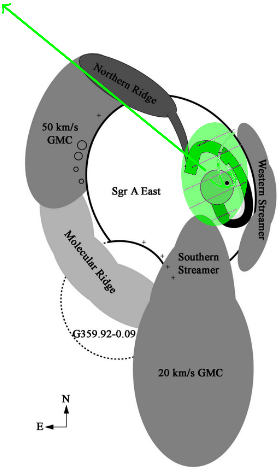

Hornstein et al. (2007)

The Sgr A complex

High-Line-Ratio (HLR) cloud
High $NH_3(6,6)/NH_3(3,3)$
Exact shape unknown
Near edge of an expanding shell?

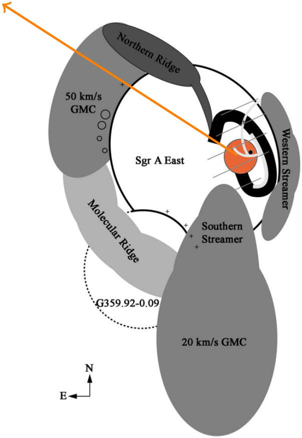

Hornstein et al. (2007)

The Sgr A complex

Sgr A West arms
Gas and dust mostly ionized

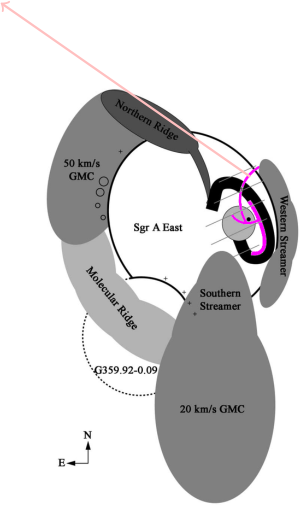

Hornstein et al. (2007)

The Sgr A complex

Sgr A* (very faint SMBH) and the S-cluster

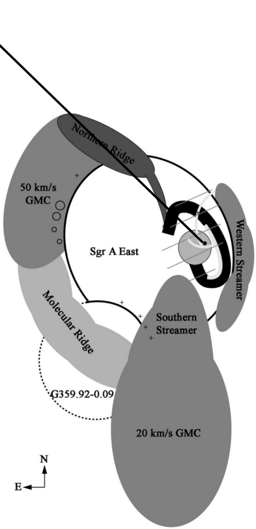

Hornstein et al. (2007)

The Sgr A complex

CircumNuclear Disk (CND)
$10^4\ M_\odot$ molecular cloud
Contains OB stars
Size: $2 \times 7\,\mathrm{pc}$
Rotate at $110\,\mathrm{km\,s^{-1}}$

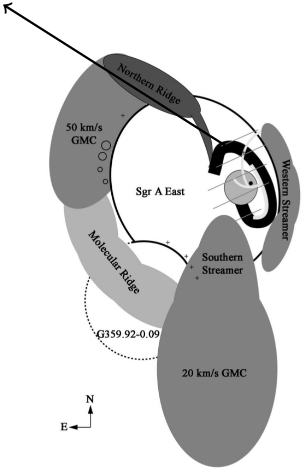

Hornstein et al. (2007)

Outline

1 The Galactic Center components

2 X-ray footprint of the CircumNuclear Disk
- The previous studies on the diffuse X-ray emission
- The X-ray diffuse emission
- Spectra
- The role of the CND

3 The X-ray emission of Sgr A* from 1999 to 2018

4 Conclusion

The previous studies on the diffuse X-ray emission

Origin of the diffuse X-ray emission

Produced by the interaction of the winds of the massive stars in the central parsec star cluster (Krabbe et al. 1991; Genzel et al. 2003).

Physical parameters of the diffuse X-ray emission

Reference	Region	Observation	Model
Baganoff et al. (2003)	$10''$	Chandra, 1999 Sept. 21	Thermal Bremsstrahlung with $\kappa T = 1.6\,\mathrm{keV}$
			Optically thin plasma model with $\kappa T = 1.3\,\mathrm{keV}$
Sakano et al. (2004)	28, 60, $100''$	XMM-Newton, 2001 Sept. 4	2T MEKAL model with $\kappa T = 1$ and $4\,\mathrm{keV}$
Quataert (2004)	$0 - 30''$	Simulation of massive stars wind	$< 2''$: $\kappa T \propto r^{-0.5}$ and $\rho \propto r^{-0.7}$ $2 - 10''$: $\kappa T \propto r^{-0.1}$ and $\rho \propto r^{-1.3}$ $10 - 30''$: $\kappa T \propto r^{-1.4}$ and $\rho \propto r^{-2.6}$

Image of the X-ray diffuse emission within $200'' \times 200''$

1999–2012 Chandra data (84 observations; 4.6 Ms)

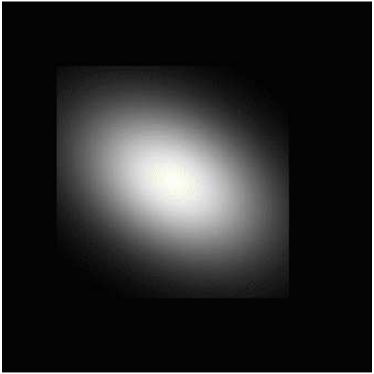

X–ray model

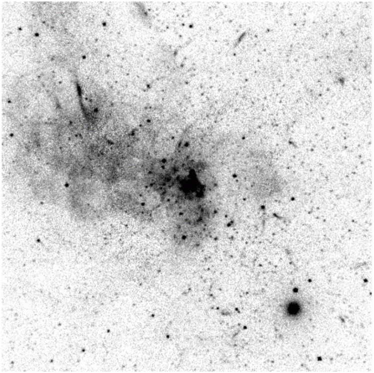

X–ray 0.5–8 keV

2' = 120'' = 4.68 pc

Image the X-ray diffuse emission within 200″ × 200″

Moser et al. (2017)

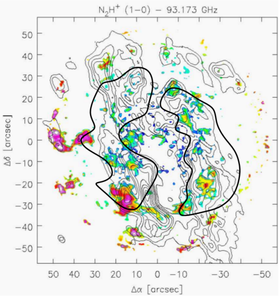

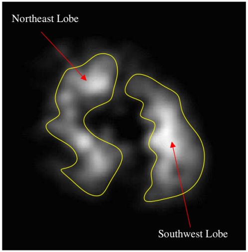

X–ray 'shadow' 0.5–8 keV

Mossoux & Eckart (2018)

Moorwood et al. (1998)

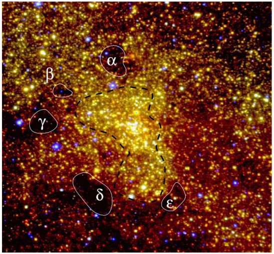

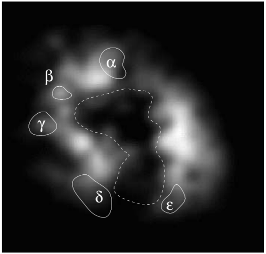

NIR 2 micron

60'' = 2.34 pc

X–ray 'shadow' 0.5–8 keV

Image the X-ray diffuse emission within 200″ × 200″

Moser et al. (2017)

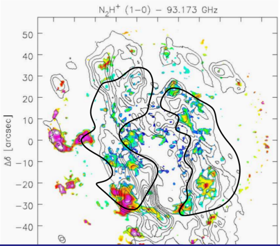

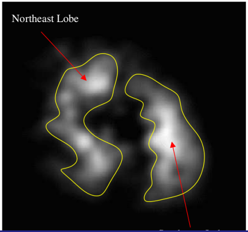

& Eckart (2018)

Two hypothesis on the role of the CND

- The CND acts as an absorbing material for the background X-ray diffuse emission;
- The CND acts as a barrier for the central plasma.

Moorwood et al.

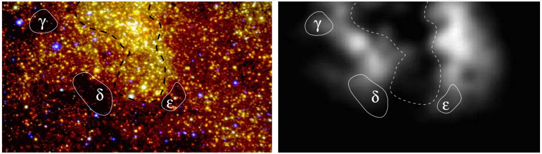

NIR 2 micron   60'' = 2.34 pc   X–ray 'shadow' 0.5–8 keV

Spectra of the X-ray diffuse emission

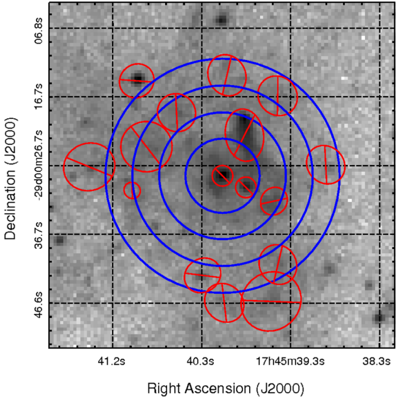

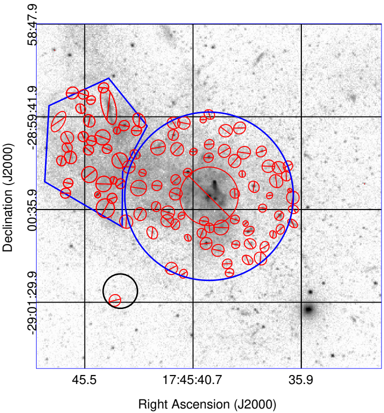

The hydrogen column density along the line of sight

The hydrogen column density along the line of sight

$$N_{\mathrm{H,LoS}} = 7.5^{+0.2}_{-0.4} \times 10^{22}\,\mathrm{cm}^{-2}$$

With the new Predehl & Schmitt (1995)'s relation (update of the ISM cross-sections and abundances):

$$N_{\mathrm{H}}/A_{\mathrm{V}} = 2.69 \times 10^{21}\,\mathrm{cm}^{-2}\,\mathrm{mag}^{-1} \text{ (Nowak et al. 2012)}.$$

$$\Rightarrow A_{\mathrm{V}} = 27.9^{+0.7}_{-1.5}\,\mathrm{mag} > 25\,\text{mag of Schödel et al. (2010)}.$$

But Predehl & Schmitt (1995)'s relation computed for sources above/below the Galactic plane and the metallicity at the Galactic center is higher
$\Rightarrow$ larger absorption of the X-rays:

$$N_{\mathrm{H}}/A_{\mathrm{V}} > 2.69 \times 10^{21}\,\mathrm{cm}^{-2}\,\mathrm{mag}^{-1}$$

Hydrogen column density, normalization and temperatures

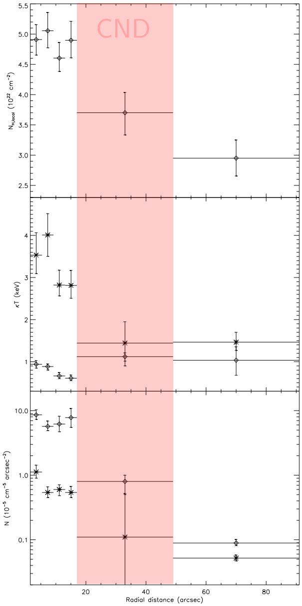

Hydrogen column density, normalization and temperatures

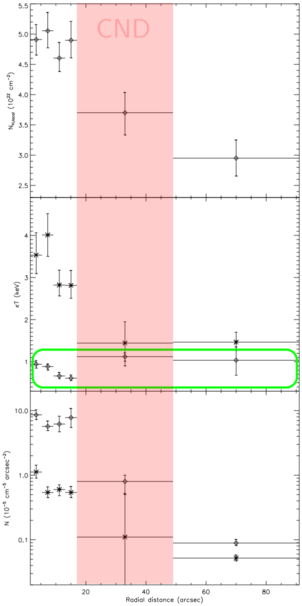

Evolution of the temperatures with the distance

Cold plasma between 1.5 and 17″:
$\kappa T = (1.4 \pm 0.2)\, r^{-0.30 \pm 0.08}$
$\rightarrow$ Extrapolation failed

Hydrogen column density, normalization and temperatures

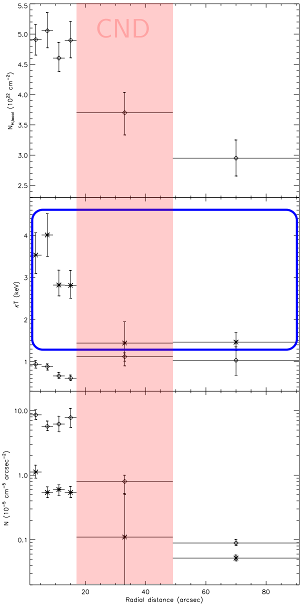

Evolution of the temperatures with the distance

Cold plasma between 1.5 and 17″:
$\kappa T = (1.4 \pm 0.2)\, r^{-0.30 \pm 0.08}$
→ Extrapolation failed

Hot plasma between 1.5 and 17″:
$\kappa T = (4.9 \pm 0.2)\, r^{-0.2 \pm 0.1}$
→ Extrapolation failed

Hydrogen column density, normalization and temperatures

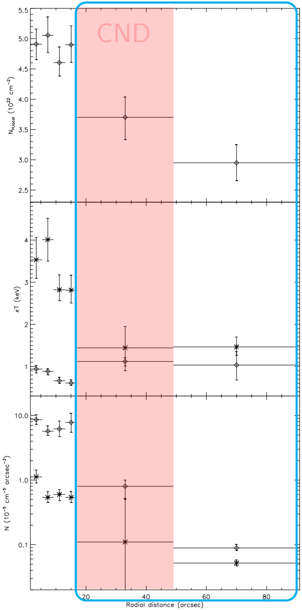

Evolution of the temperatures with the distance

Cold plasma between 1.5 and 17″:
$\kappa T = (1.4 \pm 0.2)\, r^{-0.30 \pm 0.08}$
$\rightarrow$ Extrapolation failed

Hot plasma between 1.5 and 17″:
$\kappa T = (4.9 \pm 0.2)\, r^{-0.2 \pm 0.1}$
$\rightarrow$ Extrapolation failed

$\Rightarrow$ change of the hot plasma characteristics above the inner edge of the CND

The CND: a barrier for the central plasma

Plasma "inside" the CND $\neq$ Plasma of the CND
$\Rightarrow$ absorbing material hypothesis fails.

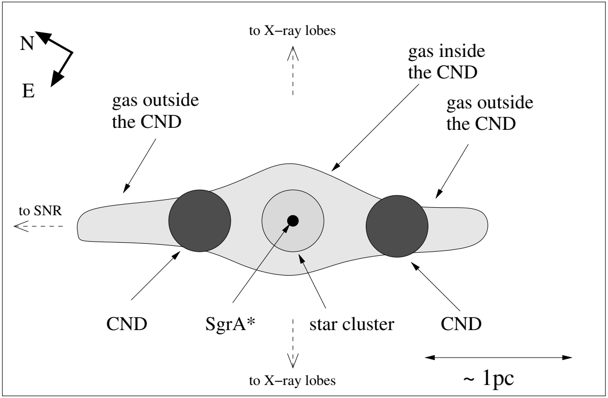

The “outside” plasma: a collimated outflow

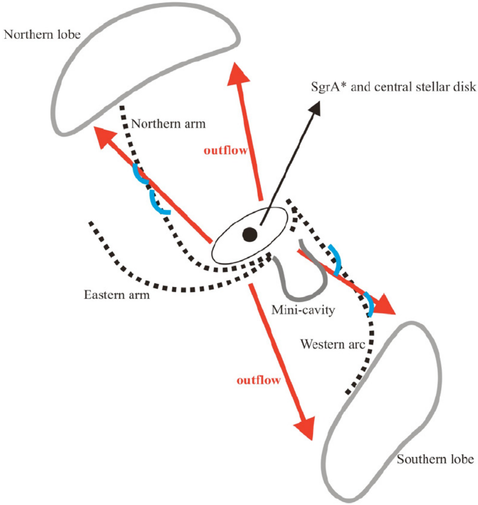

Mužić et al. (2007)

The “outside” plasma: a collimated outflow

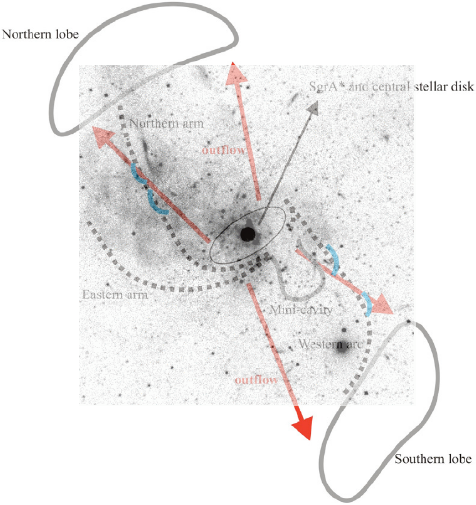

Mužić et al. (2007)

Outline

X-ray flares from Sgr A*

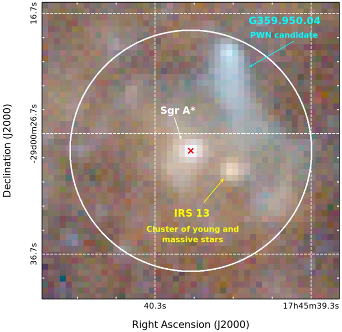

2012 Chandra *XVP* image; 1–3 keV, 3–5 keV, 5–8 keV;
non-flaring and flaring exposure times of 4.33 Ms and 190 ks;
Mossoux (2016)

X-ray flares from Sgr A*

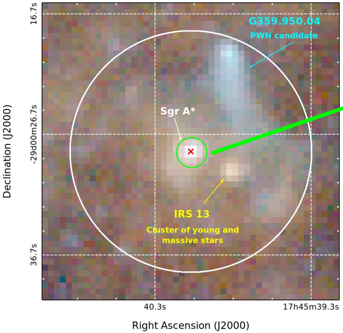

2012 Chandra *XVP* image; 1–3 keV, 3–5 keV, 5–8 keV;
non-flaring and flaring exposure times of 4.33 Ms and 190 ks;
Mossoux (2016)

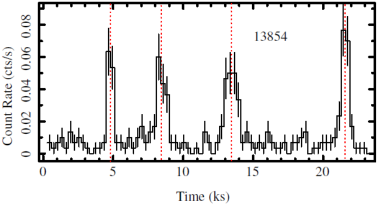

Neilsen et al. (2013)

X-ray flares from Sgr A*

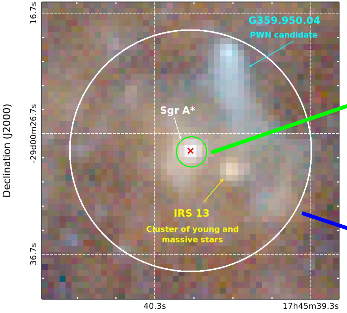

2012 Chandra *XVP* image; 1–3 keV, 3–5 keV, 5–8 keV;
non-flaring and flaring exposure times of 4.33 Ms and 190 ks;
Mossoux (2016)

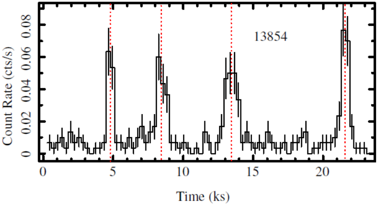

Neilsen et al. (2013)

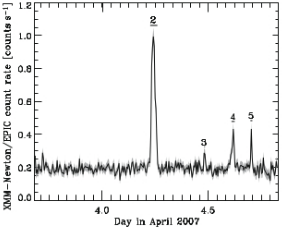

Porquet et al. (2008)

The intrinsic flare distribution

107 flares detected in 1999–2015 (Mossoux & Grosso 2017)
+ 16 flares detected in 2016–2018 (Benjamin Finociety 2019, Master Thesis)

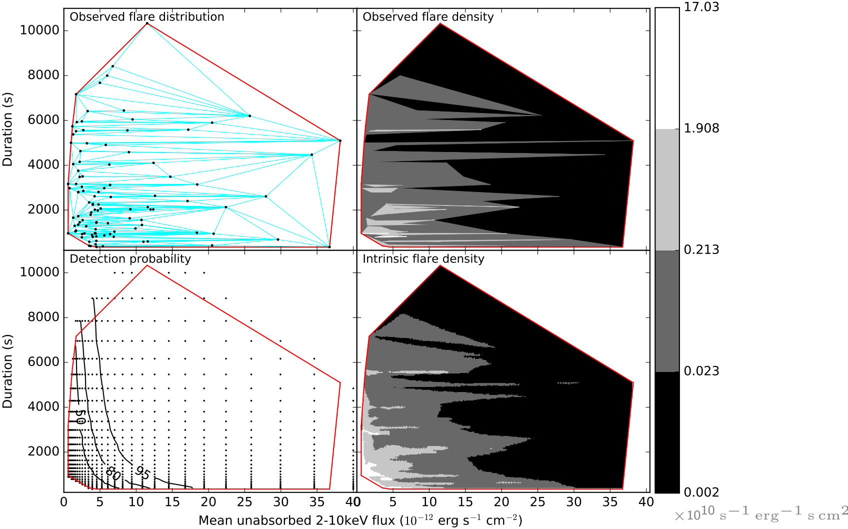

Correction from the detection efficiency

Average flare detection efficiency:

$$\eta = \frac{\int\int p_{\mathrm{facility}}(\boldsymbol{x}) \times d_{\mathrm{intr}}(\boldsymbol{x})\, d\boldsymbol{x}}{\int\int d_{\mathrm{intr}}(\boldsymbol{x})\, d\boldsymbol{x}} < 1$$

$\Rightarrow$ Correction of the observational exposures: $T_{\mathrm{corr}} = T_{\mathrm{obs}} \times \eta$

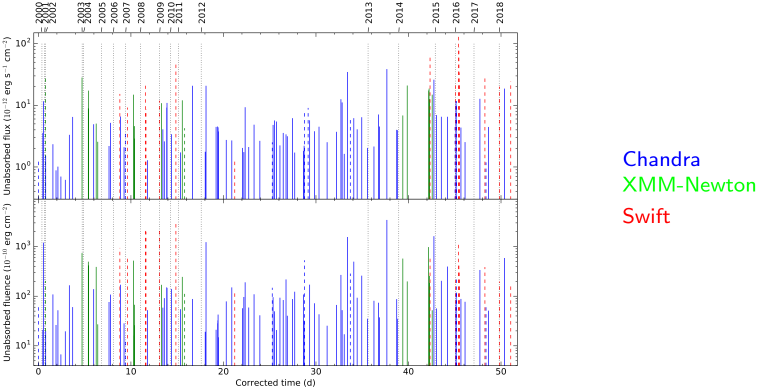

Search for flaring rate change

- Constant intrinsic flaring rate: 2.4 ± 0.2 flares per day.
- Search for flux thresholds:
  $\rightarrow$ top-to-bottom: the brightest flare is removed;
  $\rightarrow$ bottom-to-top: the faintest flare is removed.
- Search for fluence thresholds:
  $\rightarrow$ top-to-bottom: the most energetic flare is removed;
  $\rightarrow$ bottom-to-top: the less energetic flare is removed.

Search for a flux threshold

	Flux $(10^{-12}\,\mathrm{erg\,s^{-1}\,cm^{-2}})$	Date of the change point	First block (Flare per day)	Second block (Flare per day)	Significance (%)
Top-to-bottom	< 6.4	2013 May 25–July 27	1.7 ± 0.2	0.5 ± 0.2	99.9
Bottom-to-top	> 6.4	2014 Apr. 02–Aug. 30	0.7 ± 0.1	2.3 ± 0.5	97.0

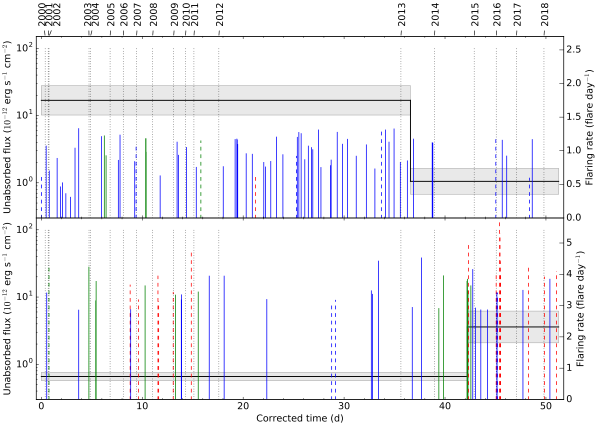

Search for a fluence threshold

No change of flaring rate found!

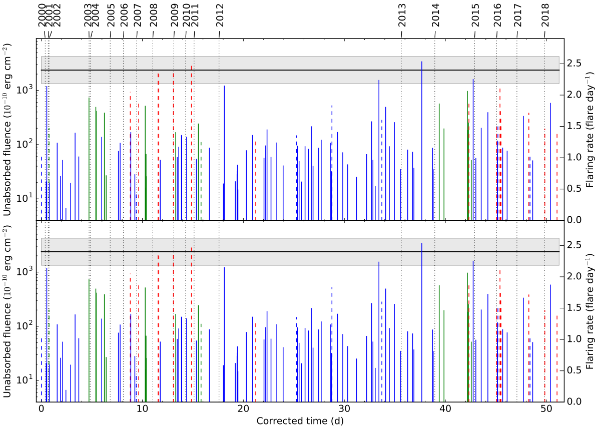

Mechanisms creating such a change

- Change in the magnetic flux in synchroton radiation (Yuan et al. 2003):
  $B \propto \dot{M}^{0.5} \propto F \rightarrow$ Change in the flux distribution
  $t_{\mathrm{f}} \propto B^{-3/2} \rightarrow$ No change in the fluence distribution
- Tidal disruption of asteroids (Zubovas et al. 2012)$\longrightarrow$ Change of the energy distribution of emitting particles:
  $\dot{N} \sim 8\, m_5\, L_{34}^{\frac{q+1}{3}}\ \mathrm{day}^{-1}$

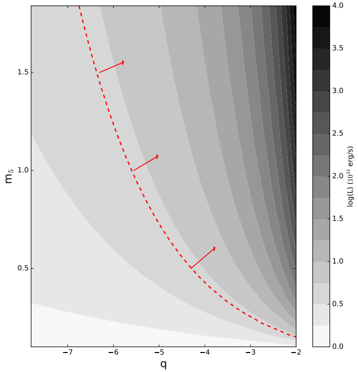

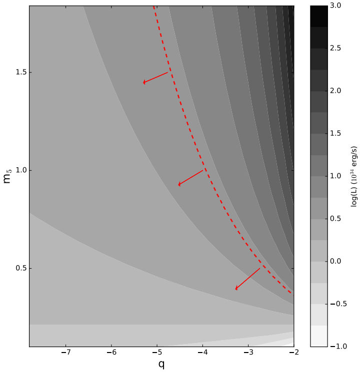

Mechanisms creating such a change

- Change in the magnetic flux in synchroton radiation (Yuan et al. 2003):
  $B \propto \dot{M}^{0.5} \propto F \rightarrow$ Change in the flux distribution
  $t_{\mathrm{f}} \propto B^{-3/2} \rightarrow$ No change in the fluence distribution
- Tidal disruption of asteroids (Zubovas et al. 2012)$\longrightarrow$ Change of the energy distribution of emitting particles:
  $\dot{N} \sim 8\, m_5\, L_{34}^{\frac{q+1}{3}}\ \mathrm{day}^{-1}$

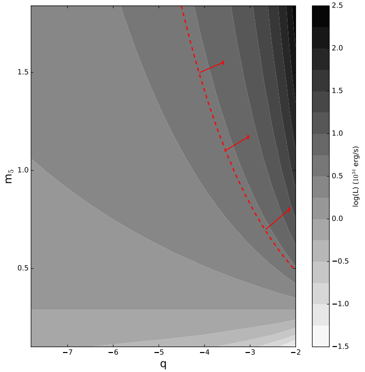

Outline

Conclusion

- $N_{\mathrm{H,LoS}} = 7.5^{+0.2}_{-0.4} \times 10^{22}\,\mathrm{cm}^{-2}$;
- New relation of Predehl & Schmitt (1995) for the Galactic Center: $N_{\mathrm{H}}/A_{\mathrm{V}} > 2.69 \times 10^{21}\,\mathrm{cm}^{-2}\,\mathrm{mag}^{-1}$;
- First image of the shadow of the CND in X-rays;
- The CND acts as a barrier for the central plasma;
- The "outside" region may correspond to the collimated outflow created by the mass-losing stars and possibly Sgr A*.
- Study of the 1999-2018 flaring rate with XMM-Newton, Chandra and Swift:
  $\Rightarrow$ The overall X-ray flaring rate is constant;
  $\Rightarrow$ Rise of the bright flaring rate & decay of the faint flaring rate;
  $\Rightarrow$ No more change of fluence distribution;
  $\Rightarrow$ Change in the magnetic flux and/or spatial distribution of flares;
  $\Rightarrow$ Rejection of the tidal disruption of asteroids to explain the overall flares.

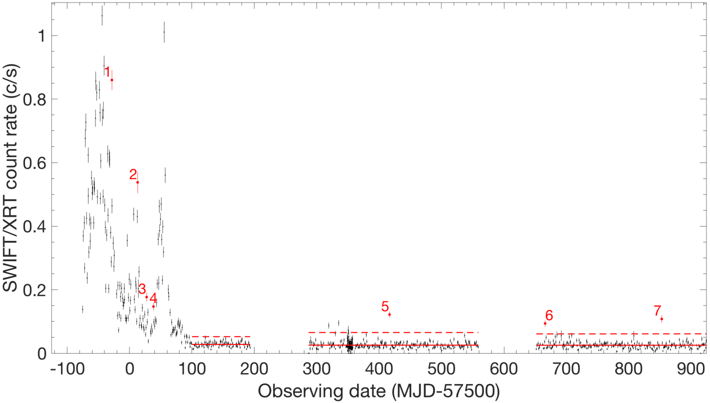
SWIFT/XRT count rate (c/s)
Observing date (MJD-57500)
0
0.2
0.4
0.6
0.8
1
-100
0
100
200
300
400
500
600
700
800
900
1
2
3
4
5
6
7

A cool accretion disk around Sgr A* (Murchikova et al. 2019)

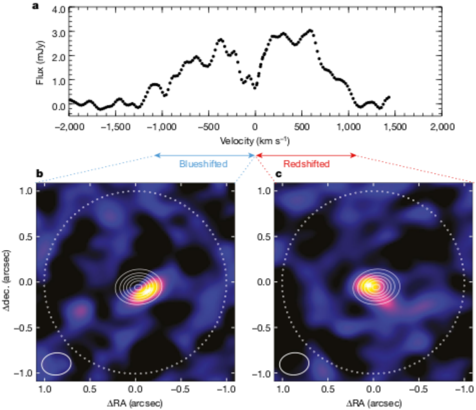

1.3 mm recombination line H30α enhanced by maser emission

A cool accretion disk around Sgr A* (Murchikova et al. 2019)

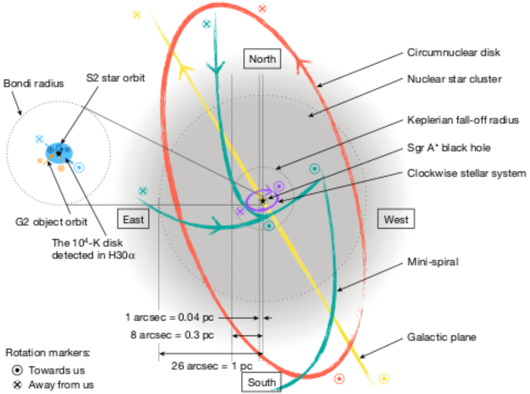

$$10^{-5} - 10^{-4}\,\mathrm{M}_\odot \text{ and } \mathrm{n_H} \sim 10^5 - 10^6\,\mathrm{cm}^{-3}$$